

Encoded quantum gates by geometric rotation on tessellations

Yixu Wang,^{1,*} Yijia Xu (许逸葭),^{2,3,†} and Zi-Wen Liu^{4,‡}

¹*Institute for Advanced Study, Tsinghua University, Beijing, 100084, China*

²*Joint Center for Quantum Information and Computer Science,
University of Maryland, College Park, Maryland 20742, USA*

³*Institute for Physical Science and Technology, University of Maryland, College Park, Maryland 20742, USA*

⁴*Yau Mathematical Sciences Center, Tsinghua University, Beijing, 100084, China*

(Dated: October 25, 2024)

We utilize the symmetry groups of regular tessellations on two-dimensional surfaces of different constant curvatures, including spheres, Euclidean planes and hyperbolic planes, to encode a qubit or qudit into the physical degrees of freedom on these surfaces. We show that the codes exhibit decent error correction properties by analysis via geometric considerations and the representation theory of the isometry groups on the corresponding surfaces. Interestingly, we demonstrate how this formalism enables the implementation of certain logical operations via geometric rotations of the surfaces. We provide a variety of concrete constructions of such codes associated with different tessellations, which give rise to different logical groups.

I. INTRODUCTION

In the pursuit of scalable quantum technologies, quantum error correction is a challenging yet essential task. Aside from the robust storage of the encoded quantum information, efficient and robust manipulation of the encoded quantum information through logical operations is also a nontrivial but crucial problem for achieving fault-tolerant quantum computing. Consequently, designing quantum error-correcting codes with desired logical gate sets emerges as a pressing problem that has garnered substantial attention, spanning a variety of important settings, including topological codes [1–7], product codes [8, 9], covariant codes [10–17], bosonic codes [18–25], dynamical codes [26–28], fusion-based quantum computing [29, 30].

In this work, we adopt a geometric perspective and study codes whose code states are extended in real space. Here, symmetries of the space can be utilized as a resource. The Gottesman–Kitaev–Preskill (GKP) code [18] utilizes the translation symmetry on flat space. We explore the rotation symmetries of two-dimensional surfaces with different curvatures and demonstrate how they enable geometric rotations to implement logical quantum gates. While codes that allow gate implementation via rotations have been explored on spheres [31–34], we approach the code construction from the new perspective of regular triangle tessellations and construct geometric codes on different curved surfaces including spheres, Euclidean planes and hyperbolic surfaces. Specifically, the connections between the group structures of the logical gate sets and the triangle groups of the tessellations underlies the construction. That is, our codes can be viewed as codes based on the representation of the logical gate sets [32, 33, 35–39]. On the other hand, our formalism utilizes lattices defined by tessellation. In this regard, our constructions also generalize the GKP codes [40, 41] based on lattices on curved spaces.

We note that some specific kinds of surface tessellation were used to construct microscopic models of holography [42–44] and quantum codes [45] in different setups in previous studies.

Specifically, we provide a versatile geometric formalism for constructing quantum codes, whose codewords are superpositions obeying patterns of surface tessellation and the logical gates correspond to rotation symmetries acting on the tessellation. By choosing different tessellations, we obtain quantum codes with different logical gate sets and error correction properties. In particular, the exotic features of hyperbolic surfaces may have striking implications for coding theory and physics. This has been seen in classical codes [46], the hyperbolic surface codes that overcome the Bravyi–Poulin–Terhal (BPT) bound [47–49], band theory for non-abelian lattices [50–53], and exotic phases of matter [54–58]. The present work provides the first examples of continuous-variable codes on hyperbolic surfaces. Especially, the infinite types of regular tessellations on hyperbolic surfaces enable us to realize a wide range of logical gate sets, including the qudit Pauli group, the single-qubit Clifford groups, the binary icosahedral group and even the single qubit universal gate set.

The paper is organized as follows. We first overview the group structure of Pauli and Clifford groups. We present their underlying connection to the triangle groups in Sec. II. In Sec. III, we set up the framework of our code construction, including the encoding map III A, the error model and its correction strategy III B. In Sec. IV, we provide several examples built from our formalism in different surfaces and tessellations, including examples on the sphere (Example 1), Euclidean plane (Examples 2, 3), and hyperbolic space (Examples 4, 5, 6). These examples exhibit the interplay among lattice symmetries, logical gate sets, and error correction. In Sec. V, we discuss the potential of our framework to realize universal logical gates.

* wangyixu@mail.tsinghua.edu.cn

† yijia@umd.edu

‡ zwliu0@tsinghua.edu.cn

II. GROUP STRUCTURE

In this work, we consider the following version of the Pauli group, whose group presentation is

$$\langle X, Z | X^2 = Z^2 = (XZ)^4 = \mathbb{1} \rangle. \quad (1)$$

The group has a centre element $XZXZ = ZXZX$, squared to identity. For a qudit of general dimension $d \geq 3$, we have $X = \sum_j |j+1\rangle\langle j|$ and $Z = \sum_j \omega^j |j\rangle\langle j|$, where $\omega = e^{i\frac{2\pi}{d}}$. The group presentation is

$$\langle X, Z | X^d = Z^d = \Omega X \Omega^{-1} X^{-1} = \Omega Z \Omega^{-1} Z^{-1} = \mathbb{1} \rangle. \quad (2)$$

Here $\Omega \equiv XZX^{-1}Z^{-1}$ is the commutator of X and Z . The last two relations mean that Ω is a central element. One can derive $\Omega^d = \mathbb{1}$ with these relations. Therefore, Ω is identified as $e^{i\frac{2\pi}{d}}\mathbb{1}$ in a unitary representation of the Pauli group. One can also derive $(XZ)^d = \mathbb{1}$ for odd integer d and $(XZ)^{2d} = \mathbb{1}$ for even integer d from Eq. (2).

There are various realizations of the single qubit Clifford group. They are equivalent up to global phases. An example presented in Ref. [36] is generated by

$$S = \begin{pmatrix} e^{i\frac{\pi}{4}} & 0 \\ 0 & e^{-i\frac{\pi}{4}} \end{pmatrix}, U = \frac{1}{\sqrt{2}} \begin{pmatrix} e^{i\frac{\pi}{4}} & e^{i\frac{\pi}{4}} \\ -e^{-i\frac{\pi}{4}} & e^{-i\frac{\pi}{4}} \end{pmatrix}. \quad (3)$$

We have $S^4 = U^3 = (US)^2 = -\mathbb{1}$. This version of the single qubit Clifford group has 48 elements. The presentation of this group can be written as

$$\langle S, U | S^8 = U^6 = (US)^4 = S^4 U^3 = S^4 (US)^2 = \mathbb{1} \rangle. \quad (4)$$

We construct codes geometrically realizing logical operations of this group in Example 5.

Regular tessellations of two-dimensional surfaces are determined by the associated triangle group. A triangle group has three generators which are reflections along each side of a triangle. Label the reflections along the corresponding sides as f_a, f_b, f_c . The triangle group $\Delta(p, q, r)$ is classified by three positive integers $\{p, q, r\}$, all greater than 1. Its presentation is

$$\langle f_a, f_b, f_c | f_a^2 = f_b^2 = f_c^2 = (f_b f_c)^p = (f_c f_a)^q = (f_a f_b)^r = \mathbb{1} \rangle. \quad (5)$$

An index-2 subgroup of the triangle group is called the proper triangle group, denoted as $\bar{\Delta}(p, q, r)$. It only contains even numbers of the reflections in the triangle group. By redefining $r_A \equiv f_b f_c, r_B \equiv f_c f_a, r_C \equiv f_a f_b = (r_A r_B)^{-1}$, its presentation is

$$\langle r_A, r_B | r_A^p = r_B^q = (r_A r_B)^r = \mathbb{1} \rangle. \quad (6)$$

Here $r_A = f_b f_c$ is the rotation around the angle A defined by sides b and c in the direction from c to b by $\frac{2\pi}{p}$. r_B and r_C have similar geometric meanings, as depicted in Figure 1.

The integers label the types of the tessellations. Their reciprocal sum is related to the curvature of the surfaces,

$$\frac{1}{p} + \frac{1}{q} + \frac{1}{r} \begin{cases} > 1 & \implies \text{sphere,} \\ = 1 & \implies \text{Euclidean plane,} \\ < 1 & \implies \text{hyperbolic plane.} \end{cases} \quad (7)$$

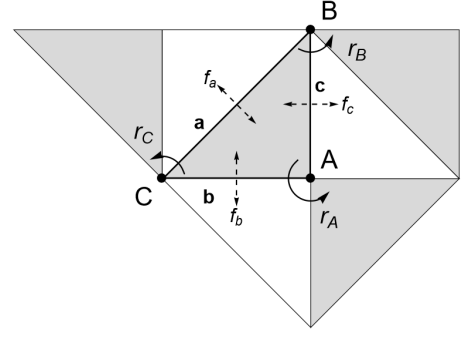


FIG. 1. The $\{2, 4, 4\}$ tessellation on the plane is used to illustrate the action of the generators of the triangle and proper triangle groups. Generators of other $\{p, q, r\}$ groups act similarly geometrically. The dashed double-arrow lines represent reflections, and the solid single-arrow lines represent rotations.

The structural similarities between the presentation of proper triangle groups (6) and the Pauli group (2) or the single qubit Clifford group (4) motivate us to realize logical qubit gates via geometric manipulations.

The presentations of the Pauli or Clifford groups have extra relations compared to their triangle group counterparts. From an algebraic perspective, imposing extra relations R is described as the quotient of the triangle group by the normal subgroup called the normal closure of R . The normal closure is generated by the generators of the form $R^{\bar{\Delta}} = \{g^{-1}rg, g \in \bar{\Delta}, r \in R\}$. Geometrically, these extra relations set identification relations to the lattice points of the tessellation, thus specifying unit cells of the lattice. The normal closure is the translation group in lattice theory and is often denoted as Γ . It plays a similar role to the stabilizer group in the non-commuting case, so we call Γ the generalized stabilizer group. The relation between the logical group G , the proper triangle group $\bar{\Delta}$, and the generalized stabilizer group Γ is

$$G = \bar{\Delta}/\Gamma. \quad (8)$$

III. GENERAL FORMALISM

A. Encoding strategy

We now explain our general framework for constructing continuous-variable quantum codes that enable geometric realizations of logical gates. The physical degree of freedom is a free massless two-dimensional boson on the corresponding surfaces. The logical degree of freedom is a qubit or a qudit, which can be understood as a virtual system that hosts the logical group actions as we shall discuss. We adopt the strategy in Ref. [36] to construct the positional configurations of the logical states. We review this formalism and specify our construction.

Let \mathcal{H}_L and \mathcal{H}_P be the logical and physical Hilbert spaces, and ρ_L and ρ be the representations of the group G acting on \mathcal{H}_L and \mathcal{H}_P , respectively. Define the linear operator $V =$

$\sum_{g \in G} \rho_L(g)^{-1} \otimes \rho(g)$. Then choose two states $|\Sigma\rangle \in \mathcal{H}_L$ and $|i\rangle \in \mathcal{H}_P$ such that $\langle \Sigma | V | i \rangle \neq 0$. The representation of the logical state $|\bar{k}\rangle \in \mathcal{H}_P$ can be written as

$$|\bar{k}\rangle \equiv \mathcal{E}(|k\rangle) \propto \sum_{g \in G} \langle \Sigma | \rho_L(g)^\dagger | k \rangle \rho(g) |\text{init}\rangle, \quad (9)$$

where $|k\rangle \in \mathcal{H}_L$ is the logical state to be encoded and $|\text{init}\rangle$ can be arbitrary state in \mathcal{H}_P . Different choices of $|\text{init}\rangle$ induce different code constructions. Indeed, $\rho(g_0)|\bar{k}\rangle = \mathcal{E}(\rho_L(g_0)|k\rangle)$.

In our constructions, $|\Sigma\rangle = |0\rangle \in \mathcal{H}_L$. The $|\text{init}\rangle$ state is taken to be a two-dimensional delta state localized at a given point p_i . We emphasize this by writing $|\text{init}\rangle = |p_i\rangle$ hereafter. $|p_i\rangle$ can be chosen arbitrarily inside or on the edges of a unit Schwarz triangle for code construction, except the vertices. If the logical unitary around a certain vertex has eigenvalue 1, $|p_i\rangle$ can be put on this vertex. In this case, instead of $|0\rangle \in \mathcal{H}_L$, we need to choose $|\Sigma\rangle = |v_1\rangle$, which is the eigenvalue 1 eigenvector of this logical unitary. The choice of the constellation points is tightly related to the code performance. It is discussed in detail in Appendix A. The group G is the designated logical group and ρ_L is its unitary representation acting on a logical qubit or qudit. The representation ρ is the quotient group in Eq. (8), acting geometrically on the state $|p_i\rangle$ as rotating the point p_i . For the spherical case, the triangle group is isomorphic to the logical group and no quotient is needed. For the planar and hyperbolic cases, each logical g can be written as $\rho(g) = \Gamma g_0 = \sum_{\gamma \in \Gamma} \gamma g_0$, for an arbitrary representative g_0 in the coset. This leads to unnormalizable states. This infinity also occurs in the exact GKP code states.

B. Error model and correction

We discuss error models on each type of surface and introduce parameters to characterize the code performance. The position error is modelled by an orientation-preserving isometric transformation of the plane and reflects the imprecision of logical operation implementations or unexpected vibration of the system. The momentum error is modelled by the eigenfunctions of the Laplacian operators on each type of surface. Physically, the eigenvalues are the kinetic energies of the modes and the errors are the unexpected energy excitations of the physical system. Mathematically, they are bases of irreducible representations of the isometry group. We denote an error operator as $\hat{E}_{r,n}$, in which r labels the representation and n labels the n -th basis of the vector space carrying the representation. In Table I, we list different types of position and momentum errors on corresponding surfaces.

The codes performance against position errors can be naturally characterized by geometric parameters. One such parameter is one-half of the minimal distance among pairs of adjacent points, which we call the resolution d_x . For the class of isometry g which transforms a point up to a finite distance, $\|p_i - gp_i\| = d_g < \infty$, if $d_g < d_x$, then the error g is correctable. The resolution d_x depends on the position of the constellation points, through the choice of $|p_i\rangle$ in Eq. (9). In Appendix A, we show how to determine the optimal resolution configuration of a given tessellation.

Then we briefly describe the general theory of the correction of position errors. To correct position error is to determine an unknown isometry. In principle, there are at most two fixed points for isometries on a sphere and at most one for isometries on an Euclidean plane or a hyperbolic plane (excluding the infinity point). Therefore, we can measure two points (three points on a sphere if the first two measurement results are antipodal) and compare their positions before and after the isometry. The unknown isometry should be solved up to an element of the generalized stabilizer group. We can then apply the inverse isometry to correct the error. Every measurement gives one position and we need to at least measure twice.

Suppose the positions of constellation points in the noiseless codewords are known, denoted as the set L . The syndrome measurement gives the positions of two points p_1^m, p_2^m of the noisy state. The error correction amounts to determining their original positions and the error g_e . We examine different ansatz of isometries that take the two positions back to one pair of points in the original configuration L . We denote all such isometries as the set $Q = \{g | gp_2^m, gp_1^m \in L\}$. If a proper probability distribution p of the group elements is given, we may use the maximal probability decoder to find the error:

$$g_e = \operatorname{argmax}_{g, g \in Q} p(g). \quad (10)$$

The analysis of the Knill–Laflamme error correction conditions [59] of momentum errors can be unified with the help of the representation theory of the isometry groups. In summary, all the pairs of $\hat{E}_{r,n}^\dagger \hat{E}_{r,n}$ satisfy the condition. For the pairs $(r_1, n_1) \neq (r_2, n_2)$, most of them also satisfy the error correction condition, exactly due to the consequence of the representation theory of the generalized stabilizer group. It is straightforward to calculate the violating pairs for the codes on the plane but harder for those on the hyperbolic plane. We collect the analysis of error correction conditions of momentum errors in Appendix B.

IV. CASE STUDIES

In the following, we introduce some representative examples of codes associated with spherical, planar, and hyperbolic tessellations derived from the above general framework, with certain groups of logical operations realized by geometric rotations. There are infinitely many different regular tessellations on the hyperbolic plane enabling us to realize a wide range of logical gate sets. We only present three examples as proof of principle. We describe each code by the type of tessellation, the generalized stabilizers, the logical operator generators, and the code performance against position and momentum errors. To lighten the notation, we take the curvature radius of both sphere and hyperbolic plane to be 1. For the Euclidean plane, the side length of the isosceles right triangle is 1. So is the side length of the equilateral triangle. We summarize the parameters and key information of all codes in

Table II. In the main text, we present the codewords configurations of the examples with a particular choice of $|p_i\rangle$. The

general codewords and their relations to other codes are given in Appendix C.

	Sphere	Euclidean plane	Hyperbolic plane
Isometry group	SO(3)	E(2)	PSL(2,ℝ)
Position errors	Rotation along any axis	Translations, rotations	Hyperbolic translations, rotations
Momentum errors	$Y_l^m(\hat{\theta}, \hat{\phi}) = P_l^m(\cos \hat{\theta})e^{im\hat{\phi}}$	$\exp(i(k_x \hat{x} + k_y \hat{y}))$	$P_{-\frac{1}{2}+is}^n(\cosh \hat{\rho})e^{in\hat{\phi}}$

TABLE I. Different types of position and momentum errors in the table. Position errors are elements of orientation-preserving isometry groups. Momentum errors are the eigenfunctions of the Laplacians of the corresponding surfaces. They are also basis of unitary representations of the isometry group.

	Example 1	Example 2	Example 3	Example 4	Example 5	Example 6
Designated logical group	Qubit Pauli	Qubit Pauli	Qutrit Pauli	\mathbb{Z}_5 qudit Pauli	Qubit Clifford	Binary icosahedral
Surface type	Sphere	Euclidean plane	Euclidean plane	Hyperbolic plane	Hyperbolic plane	Hyperbolic plane
Triangle tessellation	$\{2, 2, 4\}$	$\{2, 4, 4\}$	$\{3, 3, 3\}$	$\{5, 5, 5\}$	$\{6, 4, 8\}$	$\{4, 3, 5\}$
Generator identifications	$r_A \rightarrow Z$ $r_B \rightarrow X$ $r_C \rightarrow XZ$	$r_A \rightarrow X$ $r_B \rightarrow Z$ $r_C \rightarrow (XZ)^{-1}$	$r_A \rightarrow Z$ $r_B \rightarrow X$ $r_C \rightarrow (ZX)^{-1}$	$r_A \rightarrow Z$ $r_B \rightarrow X$ $r_C \rightarrow (ZX)^{-1}$	$r_A \rightarrow U$ $r_B \rightarrow (US)^{-1}$ $r_C \rightarrow S$	$r_A \rightarrow \Phi F^{-1}$ $r_B \rightarrow -F$ $r_C \rightarrow -\Phi^{-1}$
Extra relations	–	r_B^2	$\Omega r_A \Omega^{-1} r_A^{-1},$ $\Omega r_B \Omega^{-1} r_B^{-1}$	$\Omega r_A \Omega^{-1} r_A^{-1},$ $\Omega r_B \Omega^{-1} r_B^{-1}$	$r_B^2 r_A^3, r_B^2 r_C^4$	$r_B^2 r_A r_B^2 r_A^{-1}$
State configuration	Figure 2	Figure 3	Figure 4	Figure 6	Figure 7	Figure 8
Resolution d_x	$\frac{1}{2} \arccos \frac{1}{3}$	$\frac{1}{2}$	$\frac{\sqrt{3}}{2}$	1.6169	0.6605	0.5011

TABLE II. Different properties of the codes constructed in this work. We denote $\Omega \equiv r_B r_A r_C$, which is identified as $XZ X^{-1} Z^{-1}$, the commutator of the Pauli X and Z operator.

Example 1. First, we utilize the sphere's $\{2, 2, 4\}$ tessellation to realize a qubit code with logical Pauli operations realized by rotations. The $\bar{\Delta}(2, 2, 4)$ is isomorphic to the qubit Pauli group (1). The most general form of the logical state is presented in Eq. (C1) In Figure 2, the configuration corresponds to the specific choice $\theta_0 = \arccos \frac{1}{\sqrt{3}}, \phi_0 = \frac{\pi}{4}$. They are on the vertices of a cube. The logical operations are implemented as rotations along different axes. The logical Z is rotating around the x axis by π . The logical X is rotating around the diagonal of the x, y axis by π . The logical XZ is to rotate around the z axis counterclockwise by $\frac{\pi}{2}$.

The position error on the sphere is a rotation $R(\theta, \phi, \alpha)$ around the axis through the point (θ, ϕ) by an angle α . Therefore, for any two rotations $R_1(\theta_1, \phi_1, \alpha_1)$ and $R_2(\theta_2, \phi_2, \alpha_2)$ with $\alpha_1, \alpha_2 < \frac{1}{2} \arccos \frac{1}{3}$, the off-diagonal KL condition $\langle \bar{0} | R_2^\dagger R_1 | \bar{1} \rangle = \langle \bar{1} | R_2^\dagger R_1 | \bar{0} \rangle = 0$ is always satisfied. For the diagonal condition $\langle \bar{0} | R_2^\dagger R_1 | \bar{0} \rangle, \langle \bar{1} | R_2^\dagger R_1 | \bar{1} \rangle$, they are also 0, unless the cases in which the axis of the composite rotation $R_2^\dagger R_1$ exactly passes through one of the configuration point in logical states $|\bar{0}\rangle$ or $|\bar{1}\rangle$. However, in these special cases, because the antipodal points on the rotational axis belong to $|\bar{0}\rangle$ and $|\bar{1}\rangle$ respectively for the configuration in Figure 2, the diagonal error correction is still satisfied. Therefore, this code can correct the set of rotations $R(\theta, \phi, \alpha)$ with arbitrary (θ, ϕ)

and $\alpha < \frac{1}{2} \arccos \frac{1}{3}$.

The momentum errors are the spherical harmonics $Y_l^m := Y_l^m(\hat{\theta}, \hat{\phi}) = P_l^m(\cos \hat{\theta})e^{im\hat{\phi}}$. Because the logical $|\bar{0}\rangle$ and $|\bar{1}\rangle$ have no spatial overlap, the off-diagonal error correction conditions are always satisfied. For the diagonal part, we evaluate $\langle \bar{0} | Y_{l_1}^{m_1 \dagger} Y_{l_2}^{m_2} | \bar{0} \rangle, \langle \bar{1} | Y_{l_1}^{m_1 \dagger} Y_{l_2}^{m_2} | \bar{1} \rangle$ in Appendix B 1. The KL condition is only violated when $l_1 + l_2$ is odd and $(m_1 + m_2) \bmod 4 = 2$. The lowest uncorrectable pair of the errors is $Y_1^{0\dagger} Y_2^{\pm 2}$. Therefore, this code can correct all the momentum errors with $l = 1$.

Example 2. The next example is the $\{2, 4, 4\}$ tessellation on the Euclidean plane. Although the symmetry $\bar{\Delta}(2, 4, 4)$ is different from the qubit Pauli group, we impose the extra relation $r_B^2 = \mathbb{1}$. We obtain a two-dimensional CV code encoding a logical qubit. The logical X operation is the rotation around the marked vertex along the axis perpendicular to the surface by π . The logical Z and $(XZ)^{-1}$ are rotations around their corresponding vertices counterclockwise by $\frac{\pi}{2}$ respectively. In Figure 3, we illustrate a specific case $(x_0, y_0) = (\frac{1}{2}, \frac{1}{2})$. Here we take the vertex for the rotation $(XZ)^{-1}$ as the origin, horizontal direction as x and vertical direction as y . This code can be viewed as a two-mode GKP code encodes one logical qubit. Each direction is a single-mode GKP code encoding a

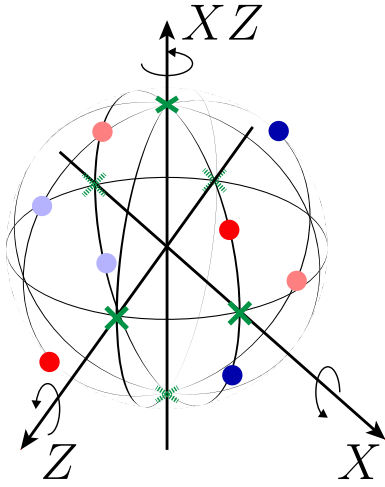


FIG. 2. The constellation of the spherical code in Example 1. The logical 0 state is superposed by the states localized at red and pink points, while logical 1 is by blue and light blue ones. The red and blue points have a coefficient of 1 while the pink and light blue ones have a coefficient of -1 .

qubit, while the full code on the plane is a 2-to-1 concatenated qubit code using the two GKP qubits. In appendix C 2 we describe in detail the stabilizers and logical operators from this point of view.

The error correction properties of this code are analogous to those of the GKP codes. For position errors of the translation type, this code can correct any translation of distance less than the resolution $d_x = \frac{1}{2}$. The momentum errors are the plane waves. We abbreviate the momentum errors, which are plane waves, as $\hat{V}_{\vec{k}} \equiv e^{ik_x \hat{x}} e^{ik_y \hat{y}}$. For a pair of errors $\hat{V}_{\vec{k}_1}^\dagger \hat{V}_{\vec{k}_2}$, write $\Delta k_x \equiv k_{x1} - k_{x2}$ and $\Delta k_y \equiv k_{y1} - k_{y2}$. The error correction condition is violated only when both $\Delta k_x, \Delta k_y$ are odd multiplicities of $\frac{\pi}{2}$. Therefore the code can correct any error with $|\vec{k}| < \frac{\sqrt{2}\pi}{4}$. The calculation for the momentum error is in Appendix B 2.

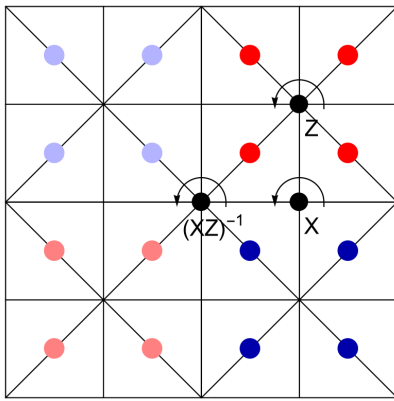


FIG. 3. The unit cell of the constellation of the Euclidean plane code. The colours represent the same as those in Figure 2. The logical operations are implemented by rotation around the corresponding vertices.

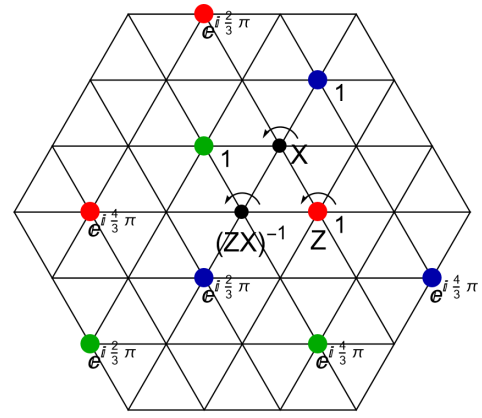


FIG. 4. The unit cell of the constellation of the qutrit code in Example 3. The red, blue and green points consist of the logical $|0\rangle, |1\rangle, |2\rangle$ states respectively. The coefficients in the superposition are labelled next to the points. The logical operations are implemented by rotation around the corresponding vertices counterclockwise by $\frac{2\pi}{3}$.

Example 3. The $\{3, 3, 3\}$ tessellation can encode a logical qutrit in the plane. As shown in Table II, the qutrit Pauli group is obtained from the $\Delta(3, 3, 3)$ group by adding an extra condition indicating $\Omega = XZX^{-1}Z^{-1}$ is a central element. The logical gate X, Z and $(ZX)^{-1}$ are implemented by rotations around the corresponding vertices by $\frac{2\pi}{3}$. Figure 4 shows one unit cell of the codewords with the choice $|p_i\rangle = |(1, 0)\rangle$. The explicit code word is shown in Eq. (C6). As described in Appendix C 3, this code has GKP-like stabilizer operators, see Eq. (C7). The GKP-like logical Z operator can also be obtained. However, the logical X operator cannot be realized by real space displacement.

For the position error of the translation type, this code corrects translation of distance less than $d_x = \frac{\sqrt{3}}{2}$. For the momentum error, the error correction condition is only violated when both $3\Delta k_x$ and $\sqrt{3}\Delta k_y$ are multiplicities of $\frac{2\pi}{3}$ but not multiplicities of 2π . It turns out this code can correct momentum errors in any direction with $|\vec{k}| < \frac{2\pi}{9}$. The detailed calculation is in Appendix B 3.

Example 4. The \mathbb{Z}_5 qudit Pauli group has presentation as in Eq. (2) with $d = 5$. It is natural to realize it on a $\{5, 5, 5\}$ lattice with extra relations, as presented in Table II. The logical gates X, Z and $(ZX)^{-1}$ are implemented by rotations around the corresponding vertices by $\frac{2\pi}{5}$. Figure 6 highlights one unit cell of the codewords if we choose $|p_i\rangle = |(b, 0)\rangle$, where $b = \text{arccosh} \frac{\cos \frac{\pi}{5} + \cos^2 \frac{\pi}{5}}{\sin^2 \frac{\pi}{5}}$ is the distance between the vertices of $(ZX)^{-1}$ and Z . For the position error of the translation type, this code corrects translation of distance less than $d_x = \frac{1}{2} \text{arccosh} \left((1 - \cos \frac{2\pi}{5}) \cosh^2 b + \cos \frac{2\pi}{5} \right) \approx 1.6169$. Because of the 5-fold rotation symmetry of the hyperbolic lattice, this code can correct any momentum error with $n < 5$.

Example 5. The group presentation of the Clifford group in Eq. (4) is analogous to the proper triangle group $\bar{\Delta}\{6, 4, 8\}$.

We can use this tessellation to construct codes with geometric logical Clifford operations. In Figure 7 we show the codeword configurations of the logical $|\bar{0}\rangle$ and $|\bar{1}\rangle$. Here we choose $|p_i\rangle = |(\frac{b}{2}, 0)\rangle$, where $b = \text{arccosh} \frac{\cos \frac{\pi}{4} + \cos \frac{\pi}{8} \cos \frac{\pi}{6}}{\sin \frac{\pi}{8} \sin \frac{\pi}{6}}$ is the distance between the vertices of S and U . The logical S gate is realized by rotation around the corresponding vertex by $\frac{\pi}{4}$, while the logical U gate is realized by rotation around the corresponding vertex by $\frac{\pi}{3}$. These gates are defined in Eq. (3). Interestingly, two logical states have positional overlap, but the relative phases guarantee that they have a zero inner product. This is analogous to the logical $|\bar{\pm}\rangle$ states of GKP code. For the position error of the translation type, this code corrects translation of distance less than $d_x = \frac{1}{2} \text{arccosh} \left((1 - \cos \frac{\pi}{4}) \cosh^2 \frac{b}{2} + \cos \frac{\pi}{4} \right) \approx 0.6605$.

Example 6. We can construct a code with the logical binary icosahedral group [37, 60] on the tessellation $\{4, 3, 5\}$. This group has 120 elements and contains non-Clifford gates. It can be generated by

$$F = \frac{e^{-i\frac{\pi}{4}}}{\sqrt{2}} \begin{pmatrix} 1 & -i \\ 1 & i \end{pmatrix}, \quad \Phi = \frac{1}{2} \begin{pmatrix} \phi_G + i\phi_G^{-1} & 1 \\ -1 & \phi_G - i\phi_G^{-1} \end{pmatrix}. \quad (11)$$

Here $\phi_G = \frac{\sqrt{5}+1}{2}$ is the golden ratio. The generators have the relations $F^3 = \Phi^5 = (\Phi F^{-1})^2 = -\mathbb{1}$. In Figure 7 we show the codeword configurations of the logical $|\bar{0}\rangle$ and $|\bar{1}\rangle$. Here we choose $|p_i\rangle = |(\frac{b}{2}, 0)\rangle$, where $b = \text{arccosh} \frac{\cos \frac{\pi}{5} + \cos \frac{\pi}{4} \cos \frac{\pi}{5}}{\sin \frac{\pi}{4} \sin \frac{\pi}{5}}$ is the distance between the vertices of $-F$ and $-\Phi^{-1}$. The logical $-F$ gate is realized by rotation around the corresponding vertex by $\frac{2\pi}{3}$, while the logical $-\Phi^{-1}$ gate is realized by rotation around the corresponding vertex by $\frac{2\pi}{5}$. These gates are defined in Eq. (3). For the position error of the translation type, this code corrects translation of distance less than $d_x = \frac{1}{2} \text{arccosh} \left((1 - \cos \frac{2\pi}{5}) \cosh^2 \frac{b}{2} + \cos \frac{2\pi}{5} \right) \approx 0.5011$.

V. UNIVERSAL GATE SET ON HYPERBOLIC SURFACES

Although the code constructions discussed above mostly focus on discrete logical groups, we note that it is possible to realize the universal single-qubit logical gate set within our formalism. Hyperbolic surfaces admit a special family of tessellations, one or two of whose labelling integers $\{p, q, r\}$ could be ∞ . For example, the $\{\infty, 2, 8\}$ tessellation has presentation $r_B^2 = r_C^8 = \mathbb{1}$. It is natural to identify r_B with the Hadamard gate H and r_C with the T gate. By imposing the extra relation $(r_B r_C^2)^3$ commutes with every generator and $(r_B r_C^2)^{24} = \mathbb{1}$, the resulting quotient of the proper triangle group is isomorphic to the universal gate set. This indicates the feasibility of using Eq. (9) to construct a code whose entire logical gate set are implemented by geometric rotations.

VI. DISCUSSION

In this work, we introduced a geometric formalism for constructing continuous variable quantum error-correcting codes

whose designated logical gate sets can be realized by geometric rotations, providing new perspectives for designing codes with desired logical gate sets. The symmetries of the tessellation lattice and the underlying surfaces play a crucial role in code construction and error correction.

Numerous directions are worth further exploring. First, the error correction protocol is worth a more comprehensive study. Specifically, we discussed the correction for position errors in Sec. III B, but the case of momentum errors has not been fully understood and should be further investigated. Second, we expect interesting geometric analogues of the Eastin–Knill theorem and its extensions [10–14, 17, 61] that characterize general limitations on logical gates. Third, we expect further studies of the geometric interpretation and physical relevance of magic in similar settings [62–64] to be fruitful. Fourth, the code state written formally in Eq. (9) is unnormalizable for the codes on the Euclidean or hyperbolic surfaces. It is interesting to study the regularized version of the code and how exact logical gates become approximate under the regularization. Fifth, generalizing our formalism to logical gates among several encoded degrees of freedom is also an important future direction for realizing universal quantum computing.

Furthermore, our formalism opens up new possibilities for experimental implementations of logical quantum computing through real-space geometric manipulations. Note that the lattices in curved manifolds have been implemented in experimental platforms [65–68]. Exploration of the application of our codes from tessellation in future quantum experiments would be worthwhile.

ACKNOWLEDGMENT

We thank Victor V. Albert for various suggestions at the early stage of this work. We thank Anthony Leverrier for sharing unpublished results. Y.W and Y.X thank Jiuci Xu for discussions about the isometry group and error correction on hyperbolic surfaces and Christophe Vuillot for discussions about GKP codes. The unit cell figures on the hyperbolic planes are generated with the assistance of the GAP package [69], the Mathematica package [70] and the data of the quotient of triangle groups [71]. Y.W. is supported by the National Natural Science Foundation of China Grant No. 12347173, China Postdoctoral Science Foundation Grant No. 2023M742003, and the Shuimu Tsinghua Scholar Program of Tsinghua University. Z.-W.L. is supported in part by a startup funding from YMSC, Tsinghua University, and NSFC under Grant No. 12475023.

Appendix A: Distances on surfaces and the resolution

In this section, we present the formula for calculating the distances of two points on the sphere and the hyperbolic plane. For the two-dimensional sphere S^2 , we conventionally embed it into the three-dimensional flat space \mathbb{R}^3 :

$$X_1 = \sin \theta \cos \phi, X_2 = \sin \theta \sin \phi, X_3 = \cos \theta, \quad X_1^2 + X_2^2 + X_3^2 = 1, \quad ds^2 = dX_1^2 + dX_2^2 + dX_3^2. \quad (\text{A1})$$

Because the sphere is a homogeneous and isotropic space, to calculate the distance of two arbitrary points on the sphere, we can always find an isometry that transforms one point to $p_1 = (\theta = 0, \phi = 0)$ and another to a certain $p_2 = (\theta = \theta_0, \phi = 0)$. In this case, it is not difficult to calculate the geodesic distance between them as θ_0 . Note that if we write the res in the embedding coordinate, we have

$$d(p_1, p_2) = \arccos \vec{X}^{(1)} \cdot \vec{X}^{(2)}, \quad (\text{A2})$$

where $\vec{X}^{(i)} = (\sin \theta \cos \phi, \sin \theta \sin \phi, \cos \theta)|_{p_i}$. Because the inner product is invariant under any isometry of the sphere, the above expression applies to arbitrary two points on the sphere.

For the hyperbolic surface, it is also convenient to embed it into $\mathbb{R}^{2,1}$.

$$X_0 = \cosh \eta, X_1 = \sinh \eta \cos \theta, X_2 = \sinh \eta \sin \theta, \quad -X_0^2 + X_1^2 + X_2^2 = -1, \quad ds^2 = -dX_0^2 + dX_1^2 + dX_2^2. \quad (\text{A3})$$

The resulting line element is $ds^2 = d\eta^2 + \sinh^2 \eta d\theta^2$. Because the hyperbolic space is also homogeneous and isotropic, we adopt the same strategy as in the sphere case to calculate the distance between two points. We first transform two points such that p_1 is at the origin, p_2 at $(\eta_0, \theta = 0)$. It is easy to calculate their distance in this case as η_0 . Writing in terms of the embedding coordinate, it is

$$d(p_1, p_2) = \text{arccosh} (-\vec{X}^{(1)} \cdot \vec{X}^{(2)}), \quad (\text{A4})$$

where $\vec{X}^{(i)} = (\cosh \eta, \sinh \eta \cos \theta, \sinh \eta \sin \theta)|_{p_i}$ and $-\vec{X}^{(1)} \cdot \vec{X}^{(2)} = X_0^{(1)} X_0^{(2)} - X_1^{(1)} X_1^{(2)} - X_2^{(1)} X_2^{(2)}$. Similar to the spherical case, because the inner product is invariant under isometry, this equation applies to any two points in the hyperbolic surface.

One special feature of the hyperbolic plane is that given the values of the three angles A, B, C of a triangle, its sides are unambiguously determined. This is not the case for the sphere or the Euclidean plane. Let the length of the sides opposite the the corresponding angles be a, b, c , we have

$$\cosh a = \frac{\cos A + \cos B \cos C}{\sin B \sin C}, \quad \cosh b = \frac{\cos B + \cos C \cos A}{\sin C \sin A}, \quad \cosh c = \frac{\cos C + \cos A \cos B}{\sin A \sin B}. \quad (\text{A5})$$

To calculate the resolution, which is one-half of the minimal distance among any pair of points, we need to get an expression of the distance between points before and after rotating around a point. This can be calculated using Eq. (A2) and (A4). For a point p_0 on the sphere, if rotated around a point j by angle α to get p_{0j} , then $\vec{X}^{(p_0)} \cdot \vec{X}^{(p_{0j})} = \sin^2 d_{0j} \cos \alpha + \cos^2 d_{0j}$, where $d_{0j} = d(p_0, p_j)$, the distance between p_0 and p_j . A similar expression in the hyperbolic case is $\vec{X}^{(p_0)} \cdot \vec{X}^{(p_{0j})} = \cosh^2 d_{0j} - \sinh^2 d_{0j} \cos \alpha$. To obtain the resolution, it is enough to evaluate the distances of the point p_i in Eq. (9) with respect to its rotated points after the rotation around A, B, C . Therefore,

$$d_x = \frac{1}{2} \min\{d(p_i, p_A), d(p_i, p_B), d(p_i, p_C)\}. \quad (\text{A6})$$

Here A, B, C are the vertices of the triangle and are usually identified with the rotation vertices of the logical operations in specific code constructions.

For a fixed tessellation, one may optimize the choice of the state $|i\rangle$ in the code construction to maximize the resolution. This is achieved by solving the optimization problem

$$p_i^{(o)} = \underset{p_i}{\text{argmax}} \min\{d(p_i, p_A), d(p_i, p_B), d(p_i, p_C)\}. \quad (\text{A7})$$

For the cases of our interest, the optimal $p_i^{(o)}$ is a solution of $d(p_i^{(o)}, p_A) = d(p_i^{(o)}, p_B) = d(p_i^{(o)}, p_C)$.

Appendix B: Analysis of the momentum error

We denote the position basis of the two-dimensional surfaces as $|x\rangle$, which is normalized to $\langle x|x'\rangle = \frac{\delta(x_1-x'_1)\delta(x_2-x'_2)}{\sqrt{h(x)}} \equiv \delta^{(2)}(x-x')$. Here $h(x)$ is the determinant of the metric evaluated at the point x . For the sphere, this is $\langle \theta, \phi|\theta', \phi'\rangle = \frac{\delta(\theta-\theta')\delta(\phi-\phi')}{\sin\theta}$. For the Euclidean plane, this is the usual $\langle x, y|x', y'\rangle = \delta(x-x')\delta(y-y')$. For the hyperbolic plane, this is $\langle \eta, \theta|\eta', \theta'\rangle = \frac{\delta(\theta-\theta')\delta(\eta-\eta')}{\sinh\eta}$. If transformed by an isometry $\rho(g)$ of the surface, the delta function is invariant under the isometry, $\delta^{(2)}(x-x') = \delta^{(2)}(\rho(g)x - \rho(g)x')$. Under the position basis, we can write the error operator as

$$\hat{E}_{r,n} = \int d^2x \sqrt{h(x)} \langle x|r, n\rangle |x\rangle \langle x|. \quad (\text{B1})$$

Here r labels the representation while n labels the basis in the representation. We match this notation with the momentum errors in Table I. For the sphere, r is the l and n is the m in Y_l^m . For the Euclidean plane, r is $\{k_x, k_y\}$ and no n is needed as the representations are one dimensional. For the hyperbolic plane, r is the s and n corresponds to the n in $P_{-\frac{1}{2}+is}^n(\cosh\hat{\rho})e^{in\hat{\phi}}$. We can write the error correction condition as

$$\langle \bar{i}|\hat{E}_{r_1, n_1}^\dagger \hat{E}_{r_2, n_2}|\bar{j}\rangle = \int d^2x \sqrt{h(x)} \langle x|r_2, n_2\rangle \langle r_1, n_1|x\rangle \langle \bar{i}|x\rangle \langle x|\bar{j}\rangle. \quad (\text{B2})$$

Following Eq. (9), we obtain

$$\begin{aligned} \langle x|\bar{j}\rangle &= \sum_{\gamma \in \Gamma} \sum_{g \in G} \langle \Sigma|\rho_L^\dagger(g)|j\rangle \langle x|\rho(\gamma g_0)|p_i\rangle = \sum_{\gamma \in \Gamma} \sum_{g \in G} \langle \Sigma|\rho_L^\dagger(g)|i\rangle \delta^{(2)}(x - \rho(\gamma g_0)p_i), \\ \langle x|\bar{j}\rangle \langle \bar{i}|x\rangle &= \sum_{\gamma_1, \gamma_2 \in \Gamma} \sum_{g_1, g_2 \in G} \langle \Sigma|\rho_L^\dagger(g_1)|j\rangle \langle i|\rho_L(g_2)|\Sigma\rangle \delta^{(2)}(x - \rho(\gamma_1 g_{01})p_i) \delta^{(2)}(x - \rho(\gamma_2 g_{02})p_i) \\ &= \sum_{\gamma \in \Gamma} \sum_{g_1, g_2 \in G} \langle \Sigma|\rho_L^\dagger(g_1)|j\rangle \langle i|\rho_L(g_2)|\Sigma\rangle \delta^{(2)}(x - \rho(\gamma_1 g_{01})p_i) \delta^{(2)}(\rho(\gamma g_{01})p_i - \rho(\gamma g_{02})p_i) \\ &= \sum_{\gamma \in \Gamma} \sum_{g_1, g_2 \in G} \langle \Sigma|\rho_L^\dagger(g_1)|j\rangle \langle i|\rho_L(g_2)|\Sigma\rangle \delta^{(2)}(x - \rho(\gamma g_{01})p_i) \delta^{(2)}(p_i - \rho(g_{01}^{-1}g_{02})p_i) \\ &= \sum_{\gamma \in \Gamma} \sum_{g_1 \in G} \sum_{g_p \in F_{p_i}} \langle \Sigma|\rho_L^\dagger(g_1)|j\rangle \langle i|\rho_L(g_1)\rho_L(g_p)|\Sigma\rangle \delta^{(2)}(x - \rho(\gamma g_{01})p_i) \delta^{(2)}(p_i - p_i) \end{aligned} \quad (\text{B3})$$

Here in the second equality the γ_1, γ_2 sums reduces to one because different unit cells do not overlap. The third equality follows from the covariance of the $\delta^{(2)}$ function under an isometry of the surface. The fourth equality follows from a change of summing variable from g_2 to g_p . The sum over g_p further reduces from G to a subgroup which keeps p_i invariant, denoted as F_{p_i} . If F_{p_i} is non trivial, because $\rho(g_p)p_i = p_i$, the delta function $\delta^{(2)}(p_i - \rho(g_p)p_i) = \delta^{(2)}(p_i - p_i)$. The sum $\sum_{g_p \in F_{p_i}} \rho_L(g_p)$ is proportional to the projector onto the common eigenvalue 1 subspace of all the group elements $\rho_L(g_p)$. As mentioned in Section III A, in this case, we choose $|\Sigma\rangle$ to be in this subspace and

$$\langle x|\bar{j}\rangle \langle \bar{i}|x\rangle = |F_{p_i}| \delta^{(2)}(p_i - p_i) \sum_{\gamma \in \Gamma} \sum_{g_1 \in G} \langle \Sigma|\rho_L^\dagger(g_1)|j\rangle \langle i|\rho_L(g_1)|\Sigma\rangle \delta^{(2)}(x - \rho(\gamma_1 g_{01})p_i). \quad (\text{B4})$$

If F_{p_i} is trivial, then $|F_{p_i}| = 1$ and the above equation also applies, but for an arbitrary $|\Sigma\rangle$.

Getting back to Eq. (B2), we obtain

$$\langle \bar{i}|\hat{E}_{r_1, n_1}^\dagger \hat{E}_{r_2, n_2}|\bar{j}\rangle = |F_{p_i}| \delta^{(2)}(p_i - p_i) \sum_{\gamma \in \Gamma} \sum_{g \in G} \langle \Sigma|\rho_L^\dagger(g)|j\rangle \langle i|\rho_L(g)|\Sigma\rangle \langle \rho(\gamma g_0)p_i|r_2, n_2\rangle \langle r_1, n_1|\rho(\gamma g_0)p_i\rangle. \quad (\text{B5})$$

If Γ is trivial, then there is no further simplification to perform and we need to evaluate Eq. (B5) with explicit data of the specific codes. This is the case of Example 1, the calculation of which is in Section B 1. If Γ is nontrivial, then it is a discrete subgroup of the full isometry group of the surface. Recall that $|r_1, n_1\rangle, |r_2, n_2\rangle$ are the basis of the unitary irreducible representation of the full isometry group. The representations r_1, r_2 are also unitary representations for the subgroup Γ , though they might not be irreducible. Fortunately, in the cases of our interests, when Γ is the translation group on the Euclidean or hyperbolic surface, the representations r_1, r_2 are also irreducible. Therefore, we can first evaluate $V_\Gamma \equiv \sum_{\gamma \in \Gamma} \rho(\gamma)^{-1} |r_2, n_2\rangle \langle r_1, n_1| \rho(\gamma)$, utilizing the Schur's lemma. There are 3 cases. The first case is $r_1 = r_2$ and $n_1 = n_2$, then $V_\Gamma = c(r_1, n_1)\mathbb{1}$. Eq. (B5) is now

$$\begin{aligned} \langle \bar{i}|\hat{E}_{r_1, n_1}^\dagger \hat{E}_{r_1, n_1}|\bar{j}\rangle &= |F_{p_i}| \delta^{(2)}(p_i - p_i) c(r_1, n_1) \sum_{g \in G} \langle \Sigma|\rho_L^\dagger(g)|j\rangle \langle i|\rho_L(g)|\Sigma\rangle \delta^{(2)}(\rho(g_0)p_i - \rho(g_0)p_i) \\ &= |F_{p_i}| |G| (\delta^{(2)}(p_i - p_i))^2 c(r_1, n_1) \delta_{i,j}. \end{aligned} \quad (\text{B6})$$

In the second equality, we use the invariance of the $\delta^{(2)}$ function and the Schur's lemma for the logical group G . Therefore, the KL condition is satisfied. The second case is that r_1, r_2 are the nonequivalent representations or n_1, n_2 are nonequivalent bases. In this case, the Schur's lemma guarantees that $\langle i | \hat{E}_{r_1, n_1}^\dagger \hat{E}_{r_2, n_2} | j \rangle = 0$ for any i, j . Therefore, the error correction condition is also satisfied. The third case is what may produce the violation of error correction condition. Because Γ is a subgroup of the full isometry group, it is possible that $|r_1, n_1\rangle, |r_2, n_2\rangle$ different bases for nonequivalent representations for the full isometry group, but become equivalent for the subgroup Γ . In this case, we can formally write Eq. (B5) as

$$\langle i | \hat{E}_{r_1, n_1}^\dagger \hat{E}_{r_1, n_1} | j \rangle = |F_{p_i}| \left(\delta^{(2)}(p_i - p_i) \right)^2 \sum_{g \in G} c(r_1, n_1, r_2, n_2, g_0 p_i) \langle \Sigma | \rho_L^\dagger(g) | j \rangle \langle i | \rho_L(g) | \Sigma \rangle. \quad (\text{B7})$$

We need to put in data of the specific codes to evaluate whether the error correction condition is violated for particular choices of $|r_1, n_1\rangle, |r_2, n_2\rangle$.

In the following, we evaluate the error correction condition explicitly for Examples 1, 2, and 3. Because the error operators are diagonal in the position basis, the two logical states have no spatial overlaps in the above examples, all the terms of the form $\langle i | \hat{E}_{r_1, n_1}^\dagger \hat{E}_{r_2, n_2} | j \rangle$ with $i \neq j$ are zero. We focus on the evaluation of terms $\langle i | \hat{E}_{r_1, n_1}^\dagger \hat{E}_{r_2, n_2} | i \rangle$.

1. Momentum error analysis of Example 1

For a generic logical state in Eq. (C1), we can calculate

$$\begin{aligned} \langle \bar{0} | Y_{l_2}^{m_2 \dagger} Y_{l_1}^{m_1} | \bar{0} \rangle &= \frac{1}{4} \left(P_{l_1}^{m_1}(\cos \theta_0) P_{l_2}^{m_2}(\cos \theta_0) e^{i(m_2 - m_1)\phi_0} + P_{l_1}^{m_1}(\cos \theta_0) P_{l_2}^{m_2}(\cos \theta_0) e^{i(m_2 - m_1)(\phi_0 + \pi)} \right. \\ &\quad \left. + P_{l_1}^{m_1}(\cos(\pi - \theta_0)) P_{l_2}^{m_2}(\cos(\pi - \theta_0)) e^{-i(m_2 - m_1)\phi_0} + P_{l_1}^{m_1}(\cos(\pi - \theta_0)) P_{l_2}^{m_2}(\cos(\pi - \theta_0)) e^{i(m_2 - m_1)(\pi - \phi_0)} \right) \\ &= \frac{1}{4} \left(P_{l_1}^{m_1}(\cos \theta_0) P_{l_2}^{m_2}(\cos \theta_0) (1 + (-1)^{m_1 + m_2}) (e^{i(m_2 - m_1)\phi_0} + e^{-i(m_2 - m_1)\phi_0} (-1)^{l_1 + l_2}) \right), \\ \langle \bar{1} | Y_{l_2}^{m_2 \dagger} Y_{l_1}^{m_1} | \bar{1} \rangle &= \frac{1}{4} \left(P_{l_1}^{m_1}(\cos \theta_0) P_{l_2}^{m_2}(\cos \theta_0) (1 + (-1)^{m_1 + m_2}) (e^{i(m_2 - m_1)(\phi_0 + \frac{\pi}{2})} + e^{-i(m_2 - m_1)(\phi_0 + \frac{\pi}{2})} (-1)^{l_1 + l_2}) \right). \end{aligned} \quad (\text{B8})$$

We used the property of the associated Legendre polynomials $P_l^m(x) = (-1)^{l+m} P_l^m(-x)$ to get the final expression. The expression for $|\bar{1}\rangle$ is different from that of $|\bar{0}\rangle$ by $\phi_0 \rightarrow \phi_0 + \frac{\pi}{2}$. We immediately see because of the factor $(1 + (-1)^{m_1 + m_2})$ and the phase difference $\frac{\pi}{2}$, $\langle \bar{0} | Y_{l_2}^{m_2 \dagger} Y_{l_1}^{m_1} | \bar{0} \rangle \neq \langle \bar{1} | Y_{l_2}^{m_2 \dagger} Y_{l_1}^{m_1} | \bar{1} \rangle$ may only occur when $(m_2 - m_1) \bmod 4 = 2$. In this case, we have

$$\langle \bar{0} | Y_{l_2}^{m_2 \dagger} Y_{l_1}^{m_1} | \bar{0} \rangle = -\langle \bar{1} | Y_{l_2}^{m_2 \dagger} Y_{l_1}^{m_1} | \bar{1} \rangle = \frac{1}{2} \left(P_{l_1}^{m_1}(\cos \theta_0) P_{l_2}^{m_2}(\cos \theta_0) (e^{i(m_2 - m_1)\phi_0} + e^{-i(m_2 - m_1)\phi_0} (-1)^{l_1 + l_2}) \right), \quad (\text{B9})$$

In the case we illustrated in Figure 2, we take $\theta_0 = \arccos \frac{1}{\sqrt{3}}$ and $\phi_0 = \frac{\pi}{4}$. In this case, we get $\langle \bar{0} | Y_{l_2}^{m_2 \dagger} Y_{l_1}^{m_1} | \bar{0} \rangle \propto (1 - (-1)^{l_1 + l_2})$. Therefore, it is only non-zero when $l_1 + l_2$ is odd. In summary, the KL condition is only violated when $l_1 + l_2$ is odd and $(m_2 - m_1) \bmod 4 = 2$. Hence, $Y_1^0 Y_2^{\pm 2}$ is the undetectable error with the smallest $|l_1| + |l_2| + |m_1| + |m_2| = 5$.

2. Momentum error analysis of Example 2

For the code of Example 2, we calculate the KL condition for a generic code state in Eq. (C2) as

$$\begin{aligned} &\langle \bar{0} | \hat{V}_{\vec{k}_2}^\dagger \hat{V}_{\vec{k}_1} | \bar{0} \rangle \\ &= \sum_{n_x, n_y \in \mathbb{Z}} e^{4i(n_x \Delta k_x + n_y \Delta k_y)} \left(4 \cos(\Delta k_x + \Delta k_y) \left(\cos(\Delta k_x - \Delta k_y + x_0 \Delta k_y - y_0 \Delta k_x) + \cos(\Delta k_x + \Delta k_y - x_0 \Delta k_x - y_0 \Delta k_y) \right) \right) \\ &= \delta_{\pi/2}(\Delta k_x) \delta_{\pi/2}(\Delta k_y) \left(4 \cos(\Delta k_x + \Delta k_y) \left(\cos(\Delta k_x - \Delta k_y + x_0 \Delta k_y - y_0 \Delta k_x) + \cos(\Delta k_x + \Delta k_y - x_0 \Delta k_x - y_0 \Delta k_y) \right) \right), \\ &\quad \cos(\Delta k_x + \Delta k_y) \langle \bar{1} | \hat{V}_{\vec{k}_2}^\dagger \hat{V}_{\vec{k}_1} | \bar{1} \rangle = \cos(\Delta k_x - \Delta k_y) \langle \bar{0} | \hat{V}_{\vec{k}_2}^\dagger \hat{V}_{\vec{k}_1} | \bar{0} \rangle, \end{aligned} \quad (\text{B10})$$

where $\Delta k_x = k_{x1} - k_{x2}$, $\Delta k_y = k_{y1} - k_{y2}$, $\delta_{\pi/2}(x) = \sum_{l \in \mathbb{Z}} \delta(x - \frac{l\pi}{2})$. Because of the delta functions, these two values are non-zero only if $\Delta k_x, \Delta k_y$ are multiplicities of $\frac{\pi}{2}$. Further evaluating the expression when $\Delta k_x, \Delta k_y$ are multiplicities of $\frac{\pi}{2}$, we see that the KL condition is violated only when $\Delta k_x, \Delta k_y$ are both odd multiplicities of $\frac{\pi}{2}$. These circumstances correspond to the logical Pauli Z operator.

3. Momentum error analysis of Example 3

For the codewords of Example 3 in Eq. (C6), the KL condition is written as

$$\begin{aligned}
\langle \bar{0} | \hat{V}_{\vec{k}_2}^\dagger \hat{V}_{\vec{k}_1} | \bar{0} \rangle &= (e^{i\Delta k_x} + e^{-2i\Delta k_x} + e^{i(-\frac{1}{2}\Delta k_x + \frac{3\sqrt{3}}{2}\Delta k_y)}) \sum_{m,n \in \mathbb{Z}} e^{i[(\frac{9}{2}\Delta k_x + \frac{3\sqrt{3}}{2}\Delta k_y)m + 3\sqrt{3}n\Delta k_y]}, \\
&= (e^{i\Delta k_x} + e^{-2i\Delta k_x} + e^{i(-\frac{1}{2}\Delta k_x + \frac{3\sqrt{3}}{2}\Delta k_y)}) \delta_{2\pi}(\frac{9}{2}\Delta k_x + \frac{3\sqrt{3}}{2}\Delta k_y) \delta_{2\pi}(3\sqrt{3}\Delta k_y), \\
\langle \bar{1} | \hat{V}_{\vec{k}_2}^\dagger \hat{V}_{\vec{k}_1} | \bar{1} \rangle &= e^{i(\frac{3}{2}\Delta k_x - \frac{\sqrt{3}}{2}\Delta k_y)} \langle \bar{0} | \hat{V}_{\vec{k}_2}^\dagger \hat{V}_{\vec{k}_1} | \bar{0} \rangle, \\
\langle \bar{2} | \hat{V}_{\vec{k}_2}^\dagger \hat{V}_{\vec{k}_1} | \bar{2} \rangle &= e^{i(-\sqrt{3}\Delta k_y)} \langle \bar{0} | \hat{V}_{\vec{k}_2}^\dagger \hat{V}_{\vec{k}_1} | \bar{0} \rangle.
\end{aligned} \tag{B11}$$

Because of the periodic delta function, $\langle \bar{0} | \hat{V}_{\vec{k}_2}^\dagger \hat{V}_{\vec{k}_1} | \bar{0} \rangle \neq 0$ only when $\frac{9}{2}\Delta k_x + \frac{3\sqrt{3}}{2}\Delta k_y = 2m\pi$ and $3\sqrt{3}\Delta k_y = 2n\pi$, $m, n \in \mathbb{Z}$. In these cases $\langle \bar{1} | \hat{V}_{\vec{k}_2}^\dagger \hat{V}_{\vec{k}_1} | \bar{1} \rangle = e^{i\frac{2\pi}{3}(m-n)} \langle \bar{0} | \hat{V}_{\vec{k}_2}^\dagger \hat{V}_{\vec{k}_1} | \bar{0} \rangle$ and $\langle \bar{2} | \hat{V}_{\vec{k}_2}^\dagger \hat{V}_{\vec{k}_1} | \bar{2} \rangle = e^{-i\frac{2\pi}{3}n} \langle \bar{0} | \hat{V}_{\vec{k}_2}^\dagger \hat{V}_{\vec{k}_1} | \bar{0} \rangle$. Therefore, the KL condition is violated when either m or n is not a multiple of 3. They are equivalent to the cases when both $3\Delta k_x$ and $\sqrt{3}\Delta k_y$ are multiplicities of $\frac{2\pi}{3}$ but not multiplicities of 2π , as stated in the main text.

Appendix C: Further discussion of code examples

In this section, we present and compare other examples of codes based on the same tessellation groups as in Example 1, 2 and 3.

1. Codes on $\{2, 2, 4\}$ tessellation

For the code constructed in Example 1, if we choose an arbitrary $|p_i\rangle = |(\theta_0, \phi_0)\rangle$ in the construction Eq. (9), the most general form of the logical states are

$$\begin{aligned}
|\bar{0}\rangle &= \frac{1}{2}(|\theta_0, \phi_0\rangle + |\pi - \theta_0, -\phi_0\rangle - |\theta_0, \pi + \phi_0\rangle - |\pi - \theta_0, \pi - \phi_0\rangle), \\
|\bar{1}\rangle &= \frac{1}{2}(|\theta_0, \phi_0 + \frac{\pi}{2}\rangle + |\pi - \theta_0, -\phi_0 + \frac{\pi}{2}\rangle - |\theta_0, -\frac{\pi}{2} + \phi_0\rangle - |\pi - \theta_0, -\frac{\pi}{2} - \phi_0\rangle).
\end{aligned} \tag{C1}$$

Here the logical Z rotates around the x axis, the logical XZ rotates around the z axis and the logical X rotates around the bisector of the x and y axes.

Example 7. Here we show another natural choice in which $\theta_0 = \frac{\pi}{2}$, $\phi_0 = 0$. The logical state configuration is illustrated in Fig. 5. The logical operations are implemented in the same manner as that in Example 1. The resolution, which is half of the minimal distance between the configuration points is $\frac{\pi}{4}$. Therefore, this code can correct any rotation with a rotation angle less than $\frac{\pi}{4}$. However, the error correction condition will be violated for those rotations whose axis passes through the states' configuration points, unlike the code in Example 1. For momentum errors, we use Eq. (B8) with $\theta_0 = \frac{\pi}{2}$, $\phi_0 = 0$. It is straightforward to find that the lowest error pair that violates the error correction condition is $Y_0^{0\dagger} Y_2^{\pm 2}$. So this code can also correct any error with $l = 1$.

Example 8. If we exclude the cases in which $|p_i\rangle$ is put on the vertices of rotation, we can solve for the maximal resolution choice of $|p_i\rangle$ of Eq. A7. The solution is $\theta_0 = \arccos \sqrt{\frac{\sqrt{2}}{4+\sqrt{2}}}$, $\phi_0 = \frac{\pi}{8}$. We depict the codeword configuration of this choice of $|p_i\rangle$ in the right panel of Figure 5. The resolution turns out to be $d_x = \frac{1}{2} \arccos \frac{\sqrt{2}}{4+\sqrt{2}} \approx 0.6533$, which is slightly larger than the case in Example 1, where $d_x = \frac{1}{2} \arccos \frac{1}{3} \approx 0.6155$. This code corrects any rotation error whose rotation angle is less than the resolution $d_x \approx 0.6533$. But similar to Example 7, it does not correct the errors when the rotation axis of $R_2^\dagger R_1$ passes through any codeword configuration point. For the momentum error, plugging $\theta_0 = \arccos \sqrt{\frac{\sqrt{2}}{4+\sqrt{2}}}$, $\phi_0 = \frac{\pi}{8}$ into Eq. (B9), we see that the error correction condition is violated when $(m_2 - m_1) \bmod 4 = 2$.

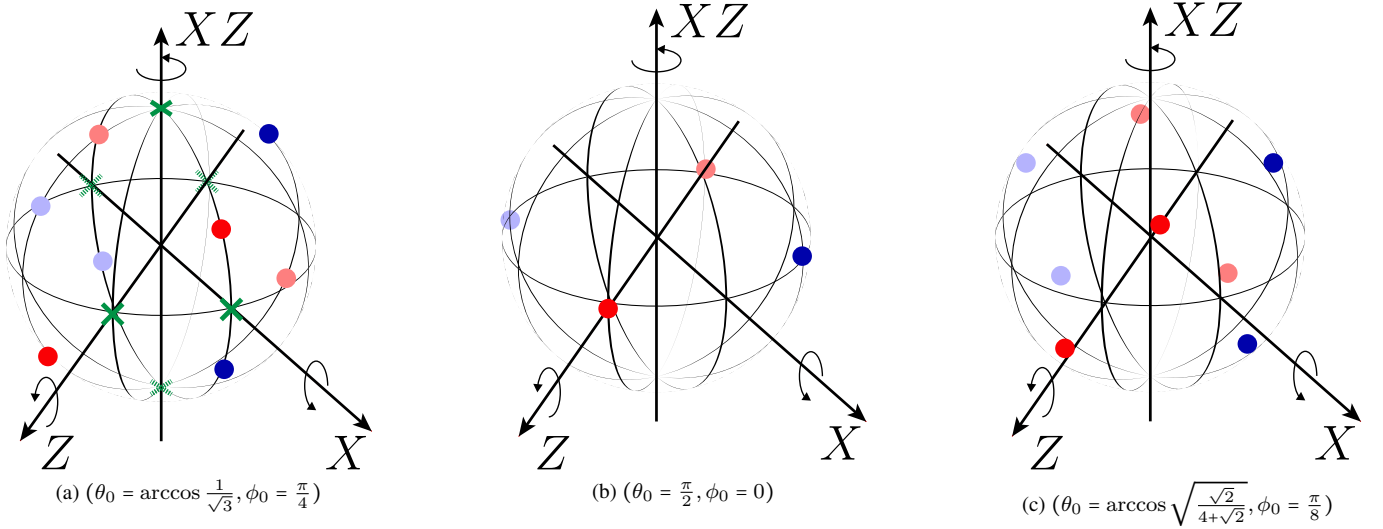


FIG. 5. This figure compares the code constructed from the same encoding map but with a different initial state $|p_i\rangle$. The constellation of the spherical code in Example 1, 7 and 8 are shown in subfigures (a), (b) and (c) respectively. The points represent the same as those in Figure 2.

2. Codes on $\{2, 4, 4\}$ tessellation

For the code construction in Figure 2, if we take the $(XZ)^{-1}$ rotation vertex as $(0, 0)$, for a generic $|p_1\rangle = |(x_0, y_0)\rangle$, the unnormalized codewords are

$$\begin{aligned}
 |\bar{0}\rangle &= \sum_{m,n \in \mathbb{Z}} | (4m + x_0, 4n + y_0) \rangle + | (4m + 2 - y_0, 4n + x_0) \rangle + | (4m + y_0, 4n + 2 - x_0) \rangle + | (4m + 2 - x_0, 4n + 2 - y_0) \rangle \\
 &\quad - | (4m - x_0, 4n - y_0) \rangle - | (4m - 2 + y_0, 4n - x_0) \rangle - | (4m - y_0, 4n - 2 + x_0) \rangle - | (4m - 2 + x_0, 4n - 2 + y_0) \rangle, \\
 |\bar{1}\rangle &= \sum_{m,n \in \mathbb{Z}} | (4m + x_0, 4n + y_0 - 2) \rangle + | (4m + 2 - y_0, 4n + x_0 - 2) \rangle + | (4m + y_0, 4n - x_0) \rangle + | (4m + 2 - x_0, 4n - y_0) \rangle \\
 &\quad - | (4m - x_0, 4n - y_0 + 2) \rangle - | (4m - 2 + y_0, 4n - x_0 + 2) \rangle - | (4m - y_0, 4n + x_0) \rangle - | (4m - 2 + x_0, 4n + y_0) \rangle.
 \end{aligned} \tag{C2}$$

As mentioned in the main text, each mode in the x or y direction is a one-dimensional GKP code. Its code words are

$$|k\rangle_{\text{GKP}} = \sum_{n \in \mathbb{Z}} |4n + 2k + \frac{1}{2}\rangle + |4n + 2k + \frac{3}{2}\rangle, \quad k \in \{0, 1\}. \tag{C3}$$

The GKP stabilizers for each mode are $\hat{S}_q = e^{i2\pi(\hat{q} - \frac{1}{2})}$ and $\hat{S}_p = e^{i4\hat{p}}$. The GKP logical operators are $X_{\text{GKP}} = e^{i2\hat{p}}$, $Z_{\text{GKP}} = \sqrt{2} \sin \frac{\pi}{2} \hat{q}$. The codewords in Eq. (C2) can be written as

$$|\bar{0}\rangle = \frac{1}{\sqrt{2}} (|0\rangle_{\text{GKP}}^{(x)} |0\rangle_{\text{GKP}}^{(y)} - |1\rangle_{\text{GKP}}^{(x)} |1\rangle_{\text{GKP}}^{(y)}), \quad |\bar{1}\rangle = \frac{1}{\sqrt{2}} (|0\rangle_{\text{GKP}}^{(x)} |1\rangle_{\text{GKP}}^{(y)} - |1\rangle_{\text{GKP}}^{(x)} |0\rangle_{\text{GKP}}^{(y)}). \tag{C4}$$

This is a 2-to-1 concatenated GKP code with stabilizers and logical operators

$$S = -X_{\text{GKP}}^{(x)} X_{\text{GKP}}^{(y)}, \quad L_X = -X_{\text{GKP}}^{(x)} = X_{\text{GKP}}^{(y)}, \quad L_Z = Z_{\text{GKP}}^{(x)} Z_{\text{GKP}}^{(y)}. \tag{C5}$$

3. Codes on $\{3, 3, 3\}$ tessellation

Taking the origin at the vertex of $(ZX)^{-1}$, the two vectors generating the translation symmetry of the lattice are $\vec{v}_1 = (0, 3\sqrt{3})$ and $\vec{v}_2 = (\frac{9}{2}, \frac{3\sqrt{3}}{2})$. The codewords can be written as

$$\begin{aligned}
|\bar{0}\rangle &= \sum_{m,n \in \mathbb{Z}} \left(|(1,0)\rangle + \omega |(-\frac{1}{2}, \frac{3\sqrt{3}}{2})\rangle + \omega^2 |(-2,0)\rangle \right) (m\vec{v}_1 + n\vec{v}_2), \\
|\bar{1}\rangle &= \sum_{m,n \in \mathbb{Z}} \left(|(1,\sqrt{3})\rangle + \omega |(-\frac{1}{2}, -\frac{\sqrt{3}}{2})\rangle + \omega^2 |(\frac{5}{2}, -\frac{\sqrt{3}}{2})\rangle \right) (m\vec{v}_1 + n\vec{v}_2), \\
|\bar{2}\rangle &= \sum_{m,n \in \mathbb{Z}} \left(|(-\frac{1}{2}, \frac{\sqrt{3}}{2})\rangle + \omega |(-2, -\sqrt{3})\rangle + \omega^2 |(1, -\sqrt{3})\rangle \right) (m\vec{v}_1 + n\vec{v}_2),
\end{aligned} \tag{C6}$$

where $\omega = e^{i\frac{2\pi}{3}}$. By $(m\vec{v}_1 + n\vec{v}_2)$ we mean translating the points in the previous parenthesis by $m\vec{v}_1 + n\vec{v}_2$. This code has GKP-like stabilizer operators. The stabilizers are

$$\hat{S}_{p,1} = e^{i3\sqrt{3}\hat{p}_y}, \hat{S}_{p,2} = e^{i(\frac{9}{2}\hat{p}_x + \frac{3\sqrt{3}}{2}\hat{p}_y)}, \hat{S}_{q,1} = e^{i\frac{4\pi}{\sqrt{3}}\hat{y}}, \hat{S}_{q,2} = e^{i(\frac{2\pi}{3}(\hat{x}-1) + \frac{2\pi}{\sqrt{3}}\hat{y})}. \tag{C7}$$

The GKP-like logical Z operator is $L_Z = e^{i\frac{4\pi}{3\sqrt{3}}\hat{y}}$ and its stabilizer equivalence. However, the logical X operator cannot be realized by real space displacement.

Appendix D: Figures of code state constellations

In this section, we collect the figures (Figures 6, 7 and 8) which illustrate the code state constellation configurations in Examples 4, 5 and 6, respectively.

-
- [1] H. Bombín, Gauge color codes: optimal transversal gates and gauge fixing in topological stabilizer codes, *New Journal of Physics* **17**, 083002 (2015).
 - [2] M. S. Kesselring, F. Pastawski, J. Eisert, and B. J. Brown, The boundaries and twist defects of the color code and their applications to topological quantum computation, *Quantum* **2**, 101 (2018).
 - [3] M. Vasmer and D. E. Browne, Three-dimensional surface codes: Transversal gates and fault-tolerant architectures, *Phys. Rev. A* **100**, 012312 (2019).
 - [4] T. Jochym-O'Connor and T. J. Yoder, Four-dimensional toric code with non-clifford transversal gates, *Phys. Rev. Res.* **3**, 013118 (2021).
 - [5] G. Zhu, T. Jochym-O'Connor, and A. Dua, Topological order, quantum codes, and quantum computation on fractal geometries, *PRX Quantum* **3**, 030338 (2022).
 - [6] G. Zhu, S. Sikander, E. Portnoy, A. W. Cross, and B. J. Brown, Non-clifford and parallelizable fault-tolerant logical gates on constant and almost-constant rate homological quantum ldpc codes via higher symmetries, arXiv preprint arXiv:2310.16982 (2023).
 - [7] M. S. Kesselring, J. C. Magdalena de la Fuente, F. Thomsen, J. Eisert, S. D. Bartlett, and B. J. Brown, Anyon condensation and the color code, *PRX Quantum* **5**, 010342 (2024).
 - [8] A. Krishna and D. Poulin, Fault-tolerant gates on hypergraph product codes, *Phys. Rev. X* **11**, 011023 (2021).
 - [9] Q. Xu, H. Zhou, G. Zheng, D. Bluvstein, J. Ataiades, M. D. Lukin, and L. Jiang, Fast and parallelizable logical computation with homological product codes, arXiv preprint arXiv:2407.18490 (2024).
 - [10] P. Faist, S. Nezami, V. V. Albert, G. Salton, F. Pastawski, P. Hayden, and J. Preskill, Continuous symmetries and approximate quantum error correction, *Phys. Rev. X* **10**, 041018 (2020).
 - [11] M. P. Woods and A. M. Alhambra, Continuous groups of transversal gates for quantum error correcting codes from finite clock reference frames, *Quantum* **4**, 245 (2020).
 - [12] S. Zhou, Z.-W. Liu, and L. Jiang, New perspectives on covariant quantum error correction, *Quantum* **5**, 521 (2021).
 - [13] A. Kubica and R. Demkowicz-Dobrzański, Using quantum metrological bounds in quantum error correction: A simple proof of the approximate eastin-knill theorem, *Phys. Rev. Lett.* **126**, 150503 (2021).
 - [14] Z.-W. Liu and S. Zhou, Quantum error correction meets continuous symmetries: fundamental trade-offs and case studies, arXiv preprint arXiv:2111.06360 (2021).
 - [15] L. Kong and Z.-W. Liu, Near-optimal covariant quantum error-correcting codes from random unitaries with symmetries, *PRX Quantum* **3**, 020314 (2022).
 - [16] Y. Yang, Y. Mo, J. M. Renes, G. Chiribella, and M. P. Woods, Optimal universal quantum error correction via bounded reference frames, *Phys. Rev. Res.* **4**, 023107 (2022).
 - [17] Z.-W. Liu and S. Zhou, Approximate symmetries and quantum error correction, *npj Quantum Information* **9**, 119 (2023).
 - [18] D. Gottesman, A. Kitaev, and J. Preskill, Encoding a qubit in an oscillator, *Phys. Rev. A* **64**, 012310 (2001).
 - [19] K. Noh and C. Chamberland, Fault-tolerant bosonic quantum error correction with the surface-gottesman-kitaev-preskill code, *Phys. Rev. A* **101**, 012316 (2020).
 - [20] B. Q. Baragiola, G. Pantaleoni, R. N. Alexander, A. Karanjai, and N. C. Menicucci, All-gaussian universality and fault tolerance with the gottesman-kitaev-preskill code, *Phys. Rev. Lett.* **123**, 200502 (2019).
 - [21] C. Calcluth, N. Reichel, A. Ferraro, and G. Ferrini, Sufficient condition for universal quantum computation using bosonic circuits, *PRX Quantum* **5**, 020337 (2024).

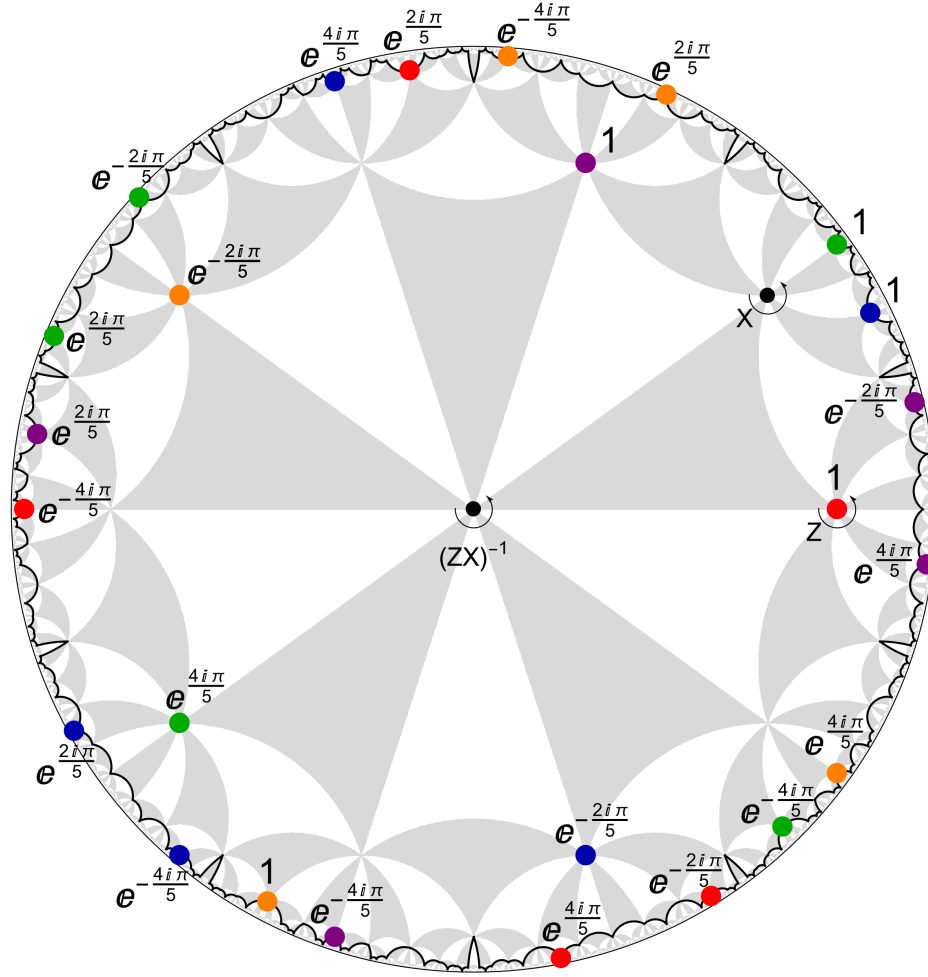


FIG. 6. The constellation of the hyperbolic code in Example 4, designed to realize \mathbb{Z}_5 qudit Pauli group via rotation. The red, blue, green, orange and purple colours label the logical $|\bar{0}\rangle$ to $|\bar{4}\rangle$ respectively. The coefficients in the superposition are labelled next to the point.

- [22] S. Krastanov, V. V. Albert, C. Shen, C.-L. Zou, R. W. Heeres, B. Vlastakis, R. J. Schoelkopf, and L. Jiang, Universal control of an oscillator with dispersive coupling to a qubit, *Phys. Rev. A* **92**, 040303 (2015).
- [23] R. W. Heeres, P. Reinhold, N. Ofek, L. Frunzio, L. Jiang, M. H. Devoret, and R. J. Schoelkopf, Implementing a universal gate set on a logical qubit encoded in an oscillator, *Nature communications* **8**, 94 (2017).
- [24] J. Guillaud and M. Mirrahimi, Repetition cat qubits for fault-tolerant quantum computation, *Phys. Rev. X* **9**, 041053 (2019).
- [25] T. Hillmann, F. Quijandría, G. Johansson, A. Ferraro, S. Gasparinetti, and G. Ferrini, Universal gate set for continuous-variable quantum computation with microwave circuits, *Phys. Rev. Lett.* **125**, 160501 (2020).
- [26] M. Davydova, N. Tantivasadakarn, S. Balasubramanian, and D. Aasen, Quantum computation from dynamic automorphism codes, *Quantum* **8**, 1448 (2024).
- [27] R. Kobayashi and G. Zhu, Cross-cap defects and fault-tolerant logical gates in the surface code and the honeycomb floquet code, *PRX Quantum* **5**, 020360 (2024).
- [28] X. Fu and D. Gottesman, Error correction in dynamical codes (2024), [arXiv:2403.04163 \[quant-ph\]](https://arxiv.org/abs/2403.04163).
- [29] S. Bartolucci, P. Birchall, H. Bombin, H. Cable, C. Dawson, M. Gimeno-Segovia, E. Johnston, K. Kieling, N. Nickerson, M. Pant, *et al.*, Fusion-based quantum computation, *Nature Communications* **14**, 912 (2023).
- [30] H. Bombin, C. Dawson, R. V. Mishmash, N. Nickerson, F. Pastawski, and S. Roberts, Logical blocks for fault-tolerant topological quantum computation, *PRX Quantum* **4**, 020303 (2023).
- [31] V. V. Albert, J. P. Covey, and J. Preskill, Robust encoding of a qubit in a molecule, *Phys. Rev. X* **10**, 031050 (2020).
- [32] J. A. Gross, Designing codes around interactions: The case of a spin, *Phys. Rev. Lett.* **127**, 010504 (2021).
- [33] S. Omanakuttan and J. A. Gross, Multispin clifford codes for angular momentum errors in spin systems, *Phys. Rev. A* **108**, 022424 (2023).
- [34] S. P. Jain, J. T. Iosue, A. Barg, and V. V. Albert, Quantum spherical codes, *Nature Physics* , 1 (2024).
- [35] A. Denys and A. Leverrier, The $2t$ -qutrit, a two-mode bosonic qutrit, *Quantum* **7**, 1032 (2023).
- [36] A. Denys and A. Leverrier, Multimode bosonic cat codes with an easily implementable universal gate set, *arXiv preprint arXiv:2306.11621* (2023).

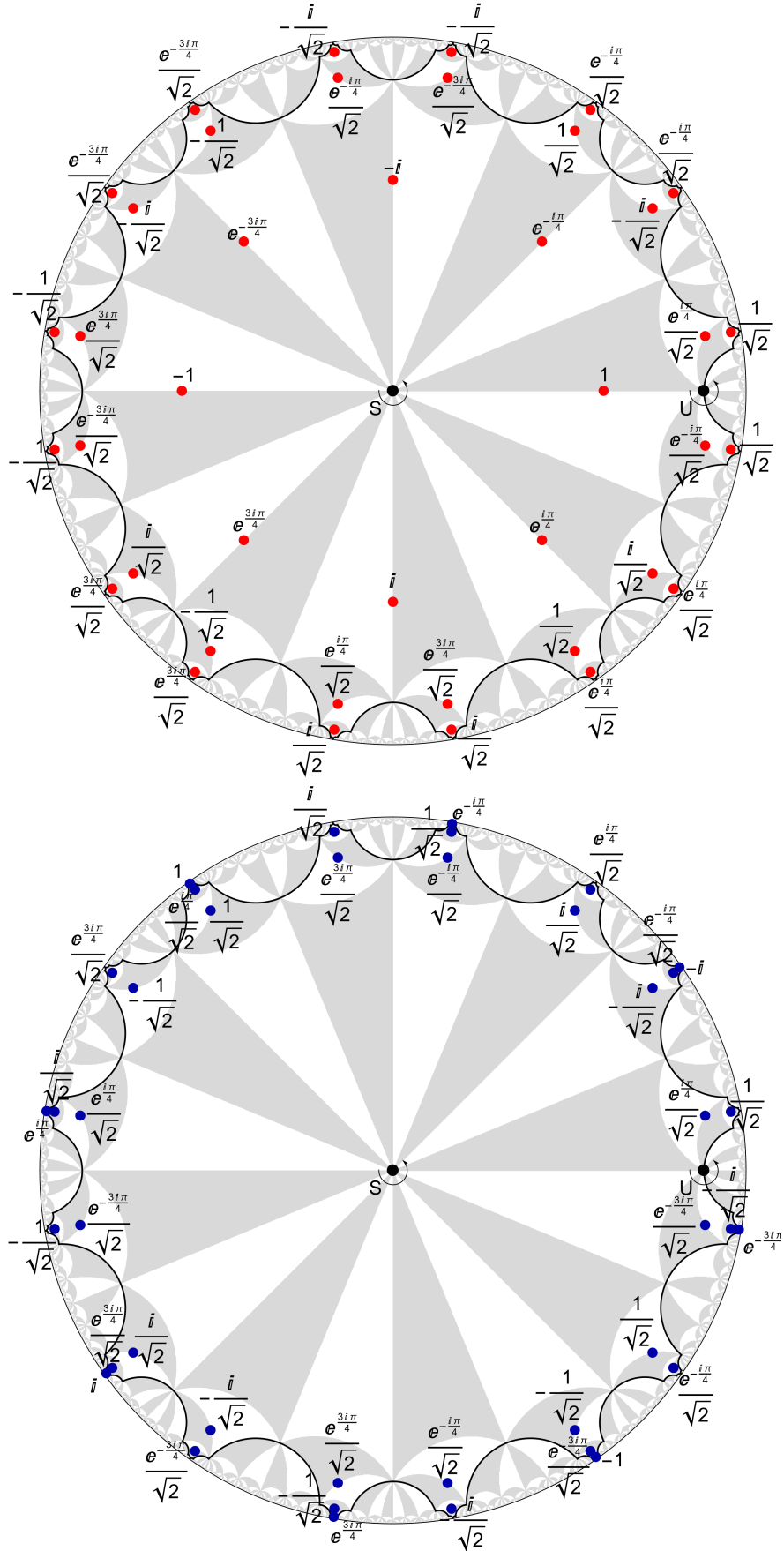


FIG. 7. The upper and lower graphs illustrate the codeword configuration of the logical $|\bar{0}\rangle$ and $|\bar{1}\rangle$ states for the construction in Example 5 respectively. Each codeword has a superposition of 40 points in one unit cell. The coefficients of the superposition are labelled next to the points.

- [37] E. Kubischta and I. Teixeira, Family of quantum codes with exotic transversal gates, *Phys. Rev. Lett.* **131**, 240601 (2023).
- [38] E. Kubischta and I. Teixeira, The not-so-secret fourth parameter of quantum codes, arXiv preprint arXiv:2310.17652 (2023).
- [39] E. Kubischta and I. Teixeira, Quantum codes and irreducible products of characters, arXiv preprint arXiv:2403.08999 (2024).
- [40] J. Conrad, J. Eisert, and F. Arzani, Gottesman-kitaev-preskill codes: A lattice perspective, *Quantum* **6**, 648 (2022).
- [41] J. Conrad, A. G. Burchards, and S. T. Flammia, Lattices, gates, and curves: Gkp codes as a rosetta stone, arXiv preprint arXiv:2407.03270 (2024).
- [42] F. Pastawski, B. Yoshida, D. Harlow, and J. Preskill, Holographic quantum error-correcting codes: Toy models for the bulk/boundary correspondence, *Journal of High Energy Physics* **2015**, 1 (2015).
- [43] L. Boyle, M. Dickens, and F. Flicker, Conformal quasicrystals and holography, *Phys. Rev. X* **10**, 011009 (2020).
- [44] L. Boyle and J. Kulp, Holographic foliations: Self-similar quasicrystals from hyperbolic honeycombs, arXiv preprint arXiv:2408.15316 (2024).
- [45] Z. Li and L. Boyle, The penrose tiling is a quantum error-correcting code, arXiv preprint arXiv:2311.13040 (2023).
- [46] E. B. da Silva, M. Firer, S. R. Costa, and R. Palazzo Jr, Signal constellations in the hyperbolic plane: A proposal for new communication systems, *Journal of the Franklin Institute* **343**, 69 (2006).
- [47] S. Bravyi, D. Poulin, and B. Terhal, Tradeoffs for reliable quantum information storage in 2d systems, *Phys. Rev. Lett.* **104**, 050503 (2010).
- [48] N. P. Breuckmann and B. M. Terhal, Constructions and noise threshold of hyperbolic surface codes, *IEEE Transactions on Information Theory* **62**, 3731 (2016).
- [49] N. P. Breuckmann, C. Vuillot, E. Campbell, A. Krishna, and B. M. Terhal, Hyperbolic and semi-hyperbolic surface codes for quantum storage, *Quantum Science and Technology* **2**, 035007 (2017).
- [50] J. Maciejko and S. Rayan, Hyperbolic band theory, *Science advances* **7**, eabe9170 (2021).
- [51] J. Maciejko and S. Rayan, Automorphic bloch theorems for hyperbolic lattices, *Proceedings of the National Academy of Sciences* **119**, e2116869119 (2022).
- [52] P. M. Lenggenhager, J. Maciejko, and T. Bzdušek, Non-abelian hyperbolic band theory from supercells, *Physical Review Letters* **131**, 226401 (2023).
- [53] I. Boettcher, A. V. Gorshkov, A. J. Kollár, J. Maciejko, S. Rayan, and R. Thomale, Crystallography of hyperbolic lattices, *Physical Review B* **105**, 125118 (2022).
- [54] P. Bienias, I. Boettcher, R. Belyansky, A. J. Kollár, and A. V. Gorshkov, Circuit quantum electrodynamics in hyperbolic space: From photon bound states to frustrated spin models, *Phys. Rev. Lett.* **128**, 013601 (2022).
- [55] A. Stegmaier, L. K. Upreti, R. Thomale, and I. Boettcher, Universality of hofstadter butterflies on hyperbolic lattices, *Phys. Rev. Lett.* **128**, 166402 (2022).
- [56] D. M. Urwyler, P. M. Lenggenhager, I. Boettcher, R. Thomale, T. Neupert, and T. c. v. Bzdušek, Hyperbolic topological band insulators, *Phys. Rev. Lett.* **129**, 246402 (2022).
- [57] A. Chen, J. Maciejko, and I. Boettcher, Anderson localization transition in disordered hyperbolic lattices, *Phys. Rev. Lett.* **133**, 066101 (2024).
- [58] T. Tummuru, A. Chen, P. M. Lenggenhager, T. Neupert, J. Maciejko, and T. Bzdušek, Hyperbolic non-abelian semimetal, *Physical Review Letters* **132**, 206601 (2024).
- [59] E. Knill and R. Laflamme, Theory of quantum error-correcting codes, *Phys. Rev. A* **55**, 900 (1997).
- [60] O. Parzanchevski and P. Sarnak, Super-golden-gates for $pu(2)$, *Advances in Mathematics* **327**, 869 (2018), special volume honoring David Kazhdan.
- [61] B. Eastin and E. Knill, Restrictions on transversal encoded quantum gate sets, *Phys. Rev. Lett.* **102**, 110502 (2009).
- [62] O. Hahn, A. Ferraro, L. Hultquist, G. Ferrini, and L. García-Álvarez, Quantifying qubit magic resource with Gottesman-Kitaev-Preskill encoding, *Phys. Rev. Lett.* **128**, 210502 (2022).
- [63] L. Feng and S. Luo, Connecting continuous and discrete Wigner functions via gkp encoding, *International Journal of Theoretical Physics* **63**, 40 (2024).
- [64] O. Hahn, G. Ferrini, and R. Takagi, Bridging magic and non-gaussian resources via Gottesman-Kitaev-Preskill encoding, arXiv preprint arXiv:2406.06418 (2024).
- [65] D. Barredo, V. Lienhard, S. De Leseleuc, T. Lahaye, and A. Browaeys, Synthetic three-dimensional atomic structures assembled atom by atom, *Nature* **561**, 79 (2018).
- [66] A. J. Kollár, M. Fitzpatrick, and A. A. Houck, Hyperbolic lattices in circuit quantum electrodynamics, *Nature* **571**, 45 (2019).
- [67] P. M. Lenggenhager, A. Stegmaier, L. K. Upreti, T. Hofmann, T. Helbig, A. Vollhardt, M. Greiter, C. H. Lee, S. Imhof, H. Brand, *et al.*, Simulating hyperbolic space on a circuit board, *Nature communications* **13**, 4373 (2022).
- [68] A. Chen, H. Brand, T. Helbig, T. Hofmann, S. Imhof, A. Fritzsche, T. Kießling, A. Stegmaier, L. K. Upreti, T. Neupert, *et al.*, Hyperbolic matter in electrical circuits with tunable complex phases, *Nature Communications* **14**, 622 (2023).
- [69] P. M. Lenggenhager, J. Maciejko, and T. Bzdušek, [HyperCells: A GAP package for constructing primitive cells and supercells of hyperbolic lattices](https://github.com/patrick-lenggenhager/HyperCells) (2023), <https://github.com/patrick-lenggenhager/HyperCells>.
- [70] P. M. Lenggenhager, J. Maciejko, and T. Bzdušek, [HyperBloch: A Mathematica package for hyperbolic tight-binding models and the supercell method](https://github.com/patrick-lenggenhager/HyperBloch) (2023), <https://github.com/patrick-lenggenhager/HyperBloch>.
- [71] M. Conder, Quotients of triangle groups acting on surfaces of genus 2 to 101, <https://www.math.auckland.ac.nz/~conder/TriangleGroupQuotients101.txt> (2007).

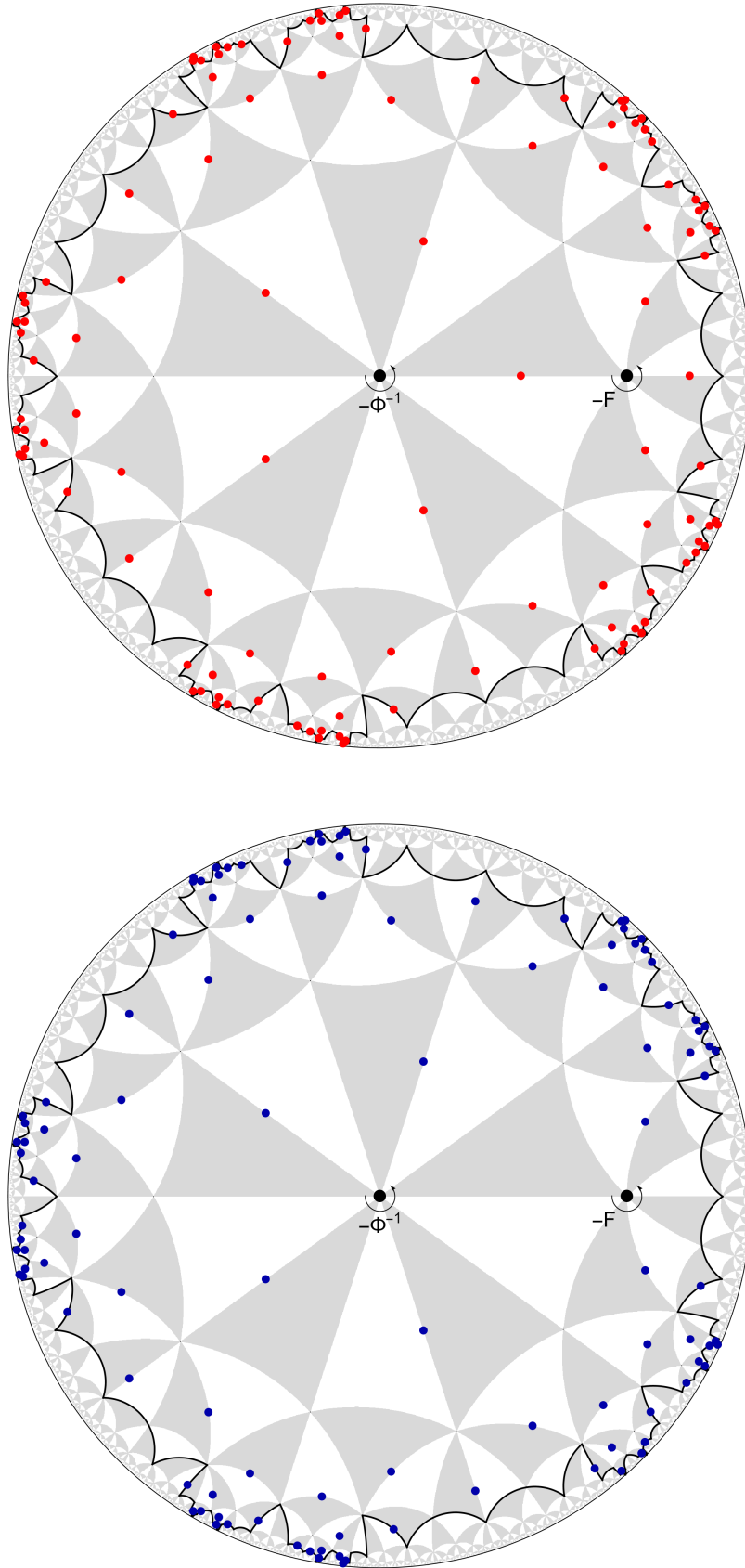


FIG. 8. The upper and lower graphs illustrate the codeword configuration of the logical $|\bar{0}\rangle$ and $|\bar{1}\rangle$ states Example 6 respectively.